



Enhancing catalytic performance, coke resistance, and stability with strontium-promoted Ni/WO₃-ZrO₂ catalysts for methane dry reforming

Ahmed Yagoub Elnour¹ · Anis Hamza Fakeeha¹ · Ahmed Aidid Ibrahim¹ · Ahmed I. Osman² · Ahmed Elhag Abasaheed¹ · Syed Farooq Adil³ · Rawesh Kumar⁴ · Ahmed S. Al-Fatesh¹

Received: 9 October 2023 / Accepted: 15 December 2023 / Published online: 24 January 2024
© The Author(s) 2024

Abstract

The first step of the DRM reaction is just the decomposition of CH₄ into CH_{4-x} ($x=1-4$). The next step comprises two steps, namely the oxidation of CH_{4-x} into syngas (by CO₂) and the self-polymerization of CH_{4-x} species. The earlier one is known as dry reforming of methane (DRM), and the latter one generates carbon deposits over the catalyst surface. In this study, we investigated the impact of 1–3

✉ Ahmed I. Osman
aosmanahmed01@qub.ac.uk

✉ Ahmed S. Al-Fatesh
aalfatesh@ksu.edu.sa

Ahmed Yagoub Elnour
aelnour@ksu.edu.sa

Anis Hamza Fakeeha
anishf@ksu.edu.sa

Ahmed Aidid Ibrahim
aididwths2011@gmail.com

Ahmed Elhag Abasaheed
abasaheed@ksu.edu.sa

Syed Farooq Adil
sfadil@ksu.edu.sa

Rawesh Kumar
kr.rawesh@gmail.com

¹ Chemical Engineering Department, College of Engineering, King Saud University, P.O. Box 800, 11421 Riyadh, Saudi Arabia

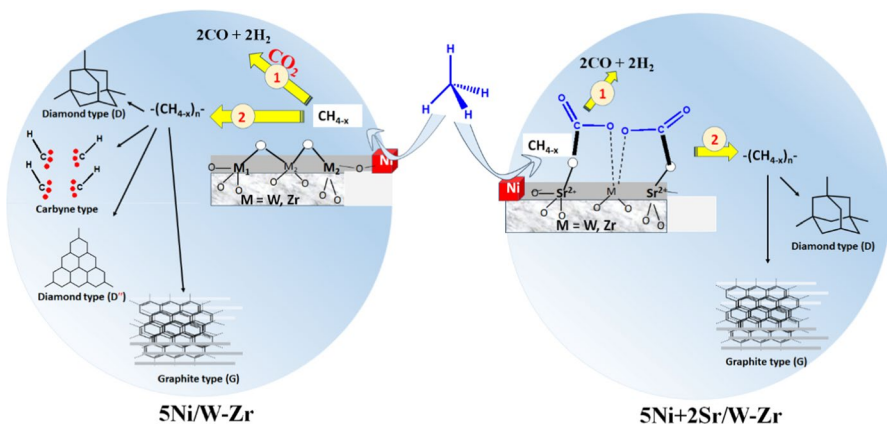
² School of Chemistry and Chemical Engineering, Queen's University Belfast, Belfast, Northern Ireland BT9 5AG, UK

³ Department of Chemistry, King Saud University, 11451 Riyadh, Saudi Arabia

⁴ Department of Chemistry, Indus University, Ahmedabad, Gujarat 382115, India

wt% Sr over Ni-based catalysts on a $\text{ZrO}_2\text{-WO}_3$ support on the catalytic activity and coke deposit. Various characterization techniques such as thermogravimetric analysis, X-ray diffraction, Raman spectroscopy, temperature-programmed oxidation, temperature-programmed reduction, and temperature-programmed desorption were used to assess the physicochemical properties of the fresh and spent catalysts. The addition of 2wt% Sr promoter significantly improves the catalyst's basicity in strong basic sites region through Sr^{2+} mediated interaction of CO_2 species as well as inhibits the deposition of carbyne type carbon. Enhanced CO_2 interaction results into the potential oxidation of carbon deposit and the highest CH_4 conversion, reaching 60% up to 470 min TOS at a reaction temperature of 700 °C.

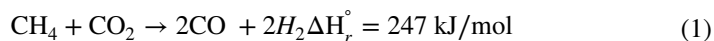
Graphical abstract



Keywords Dry reforming of methane · Syngas production · Strontium promotion · Zirconia · Tungstated zirconia

Introduction

Carbon dioxide reforming of methane, commonly referred to as dry reforming of methane, is a chemical reaction wherein methane (CH_4) and carbon dioxide (CO_2) undergo conversion into syngas, a valuable mixture comprising carbon monoxide (CO) and hydrogen (H_2). The reaction can be expressed as:



The dry reforming of methane (DRM) has emerged as a promising approach to mitigate greenhouse gas emissions. Utilizing carbon dioxide as a feedstock contributes to decreasing the release of CO_2 into the atmosphere. Furthermore, the produced syngas can serve as a valuable feedstock for synthesizing various chemicals and fuels, including methanol and Fischer–Tropsch fuels [1, 2].

Despite its potential benefits, the dry reforming of methane faces certain challenges, including catalyst deactivation and carbon deposition on the catalyst surface. Researchers are actively working on developing more efficient catalysts and optimizing reaction conditions to address these issues and make the process more suitable for large-scale industrial applications. Research groups achieved coke resistance by proper synthetic strategy, the confinement of active sites in the pore channels [3] and the use of suitable promoters. The Ni catalyst supported on alumina resulted in the formation of NiAl_xO_y species, leading to stronger metal-support interaction and improved coke resistance. [4, 5]. Qin et al. used the EDTA-assisted impregnation method to disperse 4.57–5.94 nm Ni particles onto activated carbon and achieved high coke resistance [6]. Catalyst preparation of lanthana-zirconia supported Ni under Ar atmosphere resulted in relatively lower NiO mobility which surged smaller Ni particles under reductive treatment. [7]. The smaller Ni particle had a smaller diffusion path to the metal support boundary, and the carbon deposit had less time to interact over a smaller diffusion path. Quan et al. showed 8 times higher coke resistance over Mg–Al hydrotalcite supported Ni catalyst if it is prepared in the presence of citric acid [8]. There is a general trend of using basic modifiers such as Mg, Ba, and Ca over $\text{Ni}/\text{Al}_2\text{O}_3$ [9, 10] for coke suppression. The basic promoter interacts exclusively with CO_2 and carries out potential carbon deposit oxidation. Scandium promotion over $\text{Ni}/\text{SBA}-15$ improved the basicity as well as metal-support interaction, resulting in impressive coke resistance [11]. The high resistance to coke in ceria-promoted catalyst systems (such as Ni/SiO_2 and $\text{Ni}/\text{WO}_3\text{-ZrO}_2$) is due to an increased concentration of active oxygen and the potential oxidation of coke deposits [12, 13]. The high coke resistance over Pr-promoted $\text{Ni}/\text{Al}_2\text{O}_3$ was due to stronger metal-support interaction as well as oxidation of coke by PrO_2 itself [14]. Promoting iron addition over MgO-supported Ni catalyst improved oxyphilicity and oxygen coverage, facilitating soft carbon formation, oxidation, and high coke resistance [15]. These efforts aim to enhance the overall performance and economic viability of the dry reforming of methane as a sustainable method for reducing greenhouse gas emissions and producing valuable syngas [16, 17].

Zirconia (ZrO_2) has been widely recognized as a promising support material for the dry reforming of methane (DRM) due to its advantageous properties, including high surface area, thermal stability, and efficient oxygen mobility. Notably, catalysts supported on zirconia have demonstrated the ability to effectively inhibit carbon deposition on their surfaces during DRM reactions. The unique amphoteric nature of zirconia enables its sites to serve as Lewis bases, thereby enhancing the adsorption of CO_2 , which subsequently reacts with carbon formed on the support sites, leading to the production of carbon monoxide. Despite these encouraging features and the resistance to carbonaceous species, there remains room for further improvement in the catalytic performance of zirconia-supported catalysts for DRM applications. Ongoing research aims to optimize these catalysts to unlock their full potential and address existing limitations [18, 19].

Alternatively, the catalytic performance of zirconia in the DRM reaction can be further enhanced by tailoring its unique crystal structure. One effective approach involves the incorporation of small amounts of yttrium [20, 21], ceria [22–24], and

magnesia [25, 26], among other supports, to zirconia, which can enhance its catalytic activity and stability in DRM reactions.

Numerous researchers have highlighted the suitability of Zirconia (ZrO_2) as an excellent choice for catalyst support or promoters due to its desirable properties, including thermal stability, acidic/basic characteristics, oxidizing/reducing properties, and efficient oxygen mobility. The key advantage of ZrO_2 lies in its amphoteric nature, where Lewis base sites on the ZrO_2 surface facilitate enhanced CO_2 adsorption, effectively located on these support sites [27]. Although the carbon deposition resistance of zirconium-based catalysts is quite excellent due to their good oxygen storage capacity and reducibility, catalytic performance still needs to be improved.

Incorporating tungsten oxide (WO_3) as a zirconia modifier has been shown to positively impact catalyst activity and durability, as reported in several studies [28–30]. Nevertheless, more extensive research is required to fully comprehend the potential of tungsten-supported catalysts in the DRM reaction and to optimize their design for achieving maximum activity and stability. Overall, tungsten-supported catalysts have displayed promising results in the context of DRM and continue to be an active area of research for advancing sustainable energy production.

The primary objective of this study was to investigate the catalytic efficiency and stability of Sr-promoted Ni-based catalysts, supported on commercially available tungstated zirconia ($\text{WO}_3\text{-ZrO}_2$), for the dry reforming of methane (DRM) reaction. The catalysts were synthesized using the wet impregnation technique. The study systematically examined the impact of Sr addition on the catalytic performance, coke resistance, and stability of the promoted Ni/W-Zr catalysts. Comprehensive characterization of the prepared catalysts was performed using various analysis techniques to gain insights into their physicochemical properties and behavior during the DRM reaction.

Experimental

Materials

Nickel (II) nitrate hexahydrate, $\text{Ni}(\text{NO}_3)_2 \cdot 6\text{H}_2\text{O}$; 98%, Alfa Aesar, and strontium nitrate, $\text{Sr}(\text{NO}_3)_2$; 98%, Alfa Aesar, were used as sources for the Ni active metal, and the Sr promoter, respectively. The mixed tungsten–zirconium oxide support ($10\text{WO}_3 + \text{ZrO}_2$) was given as a gift from Daiichi Kigenso Kagaku Kogyo Co., Ltd., Osaka, Japan.

Catalyst preparation

The wet impregnation process was employed to prepare the catalysts that were used in this study. The required amounts of each precursor were dissolved in 10 ml of distilled water and mixed thoroughly to obtain a homogeneous solution. Subsequently, 1 g of the $\text{WO}_3\text{-ZrO}_2$ support was added slowly. The solution was stirred under heat until a slurry was formed. The catalyst was then placed in an oven and kept overnight at

120 °C for drying. Afterward, the dyed catalyst was calcined at 600 °C for 3 h with a heating rate of 3 °C/min. Finally, the calcined catalysts were ground into powder and labeled as 5Ni + xSr/WO₃-ZrO₂ for subsequent usage, where (x) represents the Sr loading percentage (x = 0, 1, 2, and 3). The Ni loading percentage was fixed at 5% for all the catalyst samples.

Catalyst characterization

Different characterization techniques were used to elaborate on the physico-chemical properties of the as-prepared and spent catalyst samples. These techniques include BET physisorption, temperature-programmed reduction (TPR), CO₂-temperature-programmed desorption (TPD), X-ray diffraction (XRD), temperature-programmed oxidation (TPO), thermogravimetric analysis (TGA), transmission electron microscopy (TEM), Raman spectroscopy and Fourier transform infrared spectroscopy (FTIR). A detailed description of performed characterizations is supplied in supporting information.

Activity testing

The catalytic activity of the 5Ni + xSr/W-Zr catalysts was performed in a stainless steel, vertically fixed tubular reactor (PID Eng. & Tech Micro Activity Reference, 9.1 mm i.d. and 30 cm long) at 700 °C and under atmospheric conditions. In each run, 100 mg of the catalyst was well placed over glass wool. A K-type stainless sheathed thermocouple, positioned axially in the center of the catalyst bed, was used to monitor the temperature of the reactor. Before the tests, samples were reduced at a temperature of 700 °C for 60 min with a 20 ml/min flow of hydrogen gas. Equimolar CH₄ and CO₂ mixture flowed into the reactor, and N₂ was used as inert gas diluents; a volume ratio of 3:3:1 was adopted for the feed gas mixture CH₄:CO₂:N₂ with an overall volumetric flow rate of 70 ml.min⁻¹ and gas space of 48,000 ml/(h.gcat)⁻¹. A gas chromatography system (Shimadzu GC 2014) equipped with molecular sieve 5a and Porapak Q columns and a thermal conductivity detector (TCD) was used to analyze the product stream. Here, N₂ gas in the reaction feed stream is inert gas as well as an internal standard for GC. Conversions of CH₄ and CO₂ were evaluated using expressions shown in 2 and 3. Regarding the balance assessment, the mass of the total feed input and product output is measured, encompassing gases and solid products such as carbon. Elemental analysis of the feed and product was conducted to ensure balance verification, with particular emphasis on H₂, O₂, and C components. This involved weighing the catalyst before and after the reaction to gauge the carbon content. Furthermore, N₂ measurements were utilized to validate our analytical program's accuracy as a standard inert gas. The mass balance equation was computed, aiming for a % error less than 3% (Expression 4 and 5).

$$X_{CH_4}(\%) = \frac{F_{CH_4,in} - F_{CH_4,out}}{F_{CH_4,in}} \times 100 \quad (2)$$

$$X_{CO_2}(\%) = \frac{F_{CO_2,in} - F_{CO_2,out}}{F_{CO_2,in}} \times 100 \quad (3)$$

where: $F_{i,in}$ or $F_{i,out}$ are the flow rate of the component i in feed or effluent gas mixture.

$$\text{Balance} = m_{in} - m_{out}; (m = \text{H, O, C, and N}) \quad (4)$$

$$\% \text{ error} = (m_{in} - m_{out}/m_{in}) \times 100 \quad (5)$$

Results and discussion

Catalysts characterization

Textural property of catalysts

The BET surface area and pore structure properties for the different 5Ni + Sr/W + Zr catalysts are obtained by N_2 physical adsorption. Figure 1. exhibits the N_2 adsorption–desorption isotherms of the catalysts. As can be observed, all catalysts show a classical IV-type isotherm with the typical H1 hysteresis loop. This adsorption pattern depicts the mesoporous structure for all catalysts. Furthermore, the similarity of the adsorption and desorption branches between the un-promoted 5Ni/W + Zr and promoted 5Ni + xSr/W + Zr catalyst samples indicates the formation of a uniform mesoporous structure and that the incorporation of Sr promoter imparted no effect on the resultant structure. As indicated in Table 1, the unpromoted 5Ni-W + Zr catalyst has a surface area of 91 m^2/g and a pore volume of 0.221 cm^3/g . Following Sr promotion, it can be observed that the textural properties of catalyst samples almost remain intact, or in other words, incorporation of Sr promoter imparted no effect on the resultant structure.

XRD analysis

The XRD diffraction patterns of fresh calcined catalysts were adopted to assign their crystalline structure and reveal the different phases of the catalysts. As displayed in Fig. 2, it can be observed that all the catalysts exhibit almost the same diffractograms at the same 2θ angle. The characteristic peak for the tetragonal ZrO_2 phase, which typically appears at $2\theta = 30.2^\circ$, 50.2° (JCPDS 01-079-1769), was detected at 30.3° and 50.27° . Interestingly, the monoclinic phase was also detected, which is characterized by the appearance of two peaks at $2\theta \approx 28^\circ$ and 31° (JCPDS 81–1314). These monoclinic peaks were spotted at 28.3 and 31.5° [31].

Furthermore, the diffraction peaks for the cubic NiO phase were characterized by shallow peaks at 2θ values of 37.2 , 43.3 , 62.9 , and 75.0° (JCPDS 47–1049) [32]. The relatively low intensity of the NiO peaks indicates the higher dispersion of nickel oxide over all catalyst samples. Figure 2 shows that no diffraction peaks

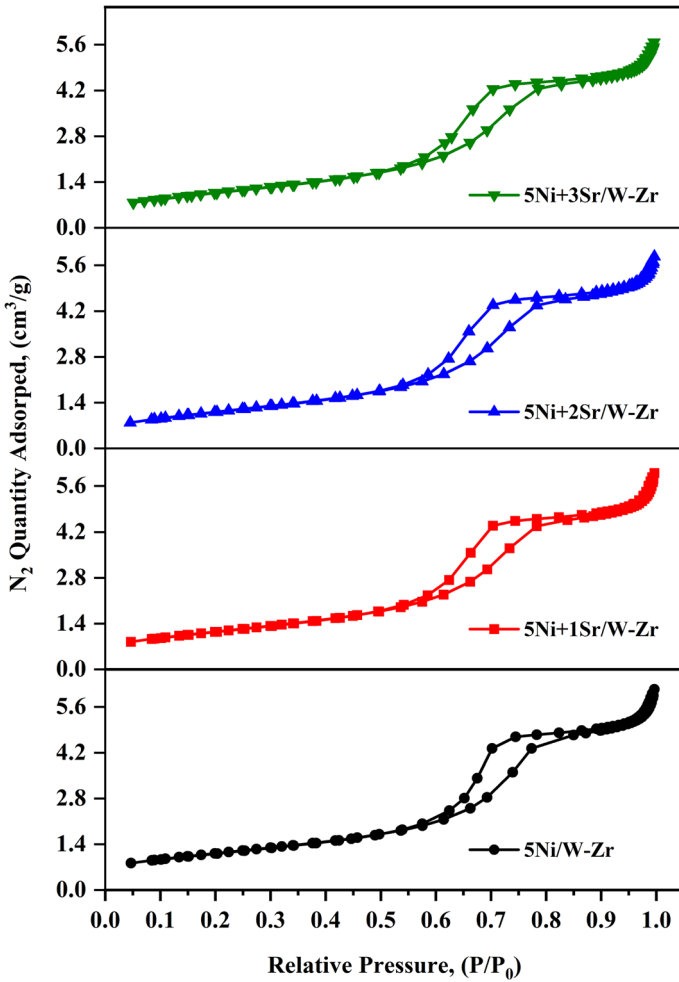


Fig. 1 N₂ adsorption–desorption isotherms of fresh calcined catalyst samples

Table 1 Textural properties (S_{BET}, D_{pore}, and V_{pore}) of the Sr-promoted 5Ni/W–Zr catalysts

Catalyst	S _{BET} , m ² /g	V _{pore} , cm ³ /g	D _{pore} , nm
5Ni/W–Zr	91.08	0.221	8.53
5Ni + 1Sr/W–Zr	93.77	0.216	8.05
5Ni + 2Sr/W–Zr	92.60	0.215	7.92
5Ni + 3Sr/W–Zr	88.70	0.209	7.89

^aS_{BET}: BET surface area; ^bV_{pore}: BJH adsorption pore volume; and ^cV_{pore}: BJH adsorption average pore width

related to strontium phases were noticed on the catalysts, which is due to the low content or high dispersion of strontium on the catalysts. Again, the possibility of mutual solubility of SrO and NiO about catalyst preparation temperature is also

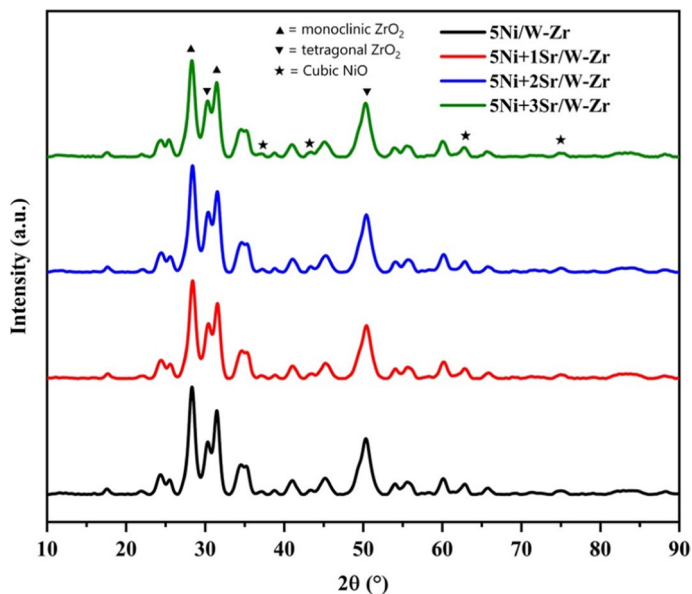


Fig. 2 XRD of fresh calcined catalyst samples

negligible [33]. That means both metaloxides, SrO and NiO, keep their identity over support.

H_2 -temperature programmed reduction (H_2 -TPR).

H_2 -TPR analysis of the as-calcined catalysts was used to examine the degree of interaction between Ni species and the surfaces of the supporting materials, as indicated by the catalysts' reducibility. All catalyst samples exhibit two separate peaks between 350 and 1000 °C, as shown in Fig. 3a, demonstrating the presence

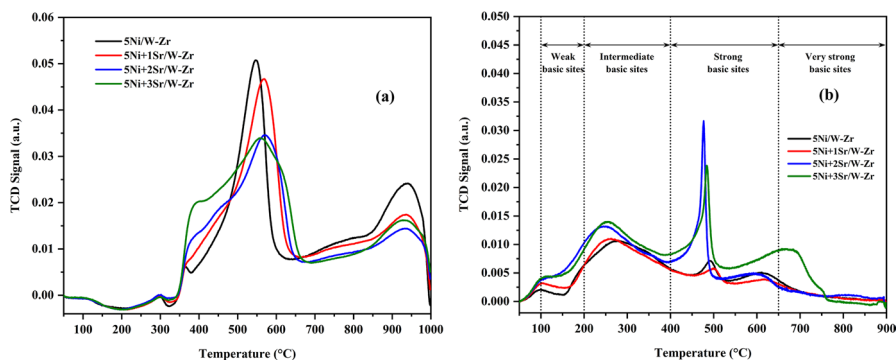


Fig. 3 H_2 -TPR (a) and CO_2 -TPD (b) profiles of the fresh calcined $5Ni+xSr/W-Zr$ ($x=0, 1, 2,$ and 3) catalysts

of nickel species with varying degrees of interaction with the W–Zr support. The reduction of the NiO phase, which is moderately linked to the W–Zr support, is carried about 550 °C under hydrogen in H₂-TPR. At the same time, the second broad peak (centered above 900 °C) is associated with the reduction of the NiO phase, which is strongly interacted with W–Zr support. This later peak at high temperatures (T > 800 °C) might also indicate the formation of NiO–ZrO₂ solid solutions [30]. Furthermore, the negative peaks in the temperature range of 100 to 300 °C may be due to the hydrogen spillover in the mesopores of W–Zr support [30]. Notably, incorporating the Sr promoter, the peak intensity of both peaks is relatively suppressed, and the reduction peak pattern is extended to a relatively lower temperature. It indicates that upon increasing Sr loading over the 5Ni/W–Zr catalyst, the catalyst attains a higher edge of reduction (Table 2).

CO₂–temperature programmed desorption (CO₂–TPD)

The CO₂-TPD profiles for the 5Ni + xSr/W–Zr (x = 0, 1, and 3) catalyst samples are demonstrated in Fig. 3(b). Four principal adsorption peaks for the catalyst samples could be recognized. These four peaks are extended across the regions of weak, medium, strong, and very strong basicity temperatures, with maxima at around 100–200, 200–400, 400–500, and 700 °C, respectively [33–35]. The catalytic performance during the DRM reaction is significantly impacted by the basicity of Ni-based catalysts, as described in the literature [36, 37]. For instance, CO₂ behaves as an acid in the DRM reaction toward the catalyst surface, which serves as a base. Since gasification of the intermediate carbon formed on the surface is made easier by the increased basicity of the catalyst, it is hypothesized that this will increase the activation of acidic CO₂ on the catalyst's surface, oxidation of carbon deposit into syngas and thereby a basic catalyst surface inhibits carbonaceous deposition [38]. This will also increase the stability of the catalyst.

Interestingly, one can observe that catalysts containing 2 and 3 wt% Sr showed the highest basicity, as indicated by the peak intensities in the region of strong basic sites. However, this trend is apparent due to the basic nature of the Sr promoter. However, the presence of very strong basic sites in the 3 wt% Sr sample, indicated by its dominant peak in the region of very strong basic sites. The intermediate strength basic sites (about 250 °C) are burned by surface hydroxyl, whereas strong basic sites (about 450 °C) are constituted by surface oxygen anion. 5Ni + 2Sr/W–Zr

Table 2 Methane conversion and deactivation factors (DF) for the Sr-promoted 5Ni/W–Zr catalysts. Reaction conditions: 700 °C, ambient pressure, and GHSV = 42,000 cm³/ (h.gcat)

Catalyst	Initial ^a	Final ^b	D.F. (%) ^c
5Ni/W–Zr	60.25	51.92	13.83
5Ni + 1Sr/W–Zr	59.16	53.79	9.08
5Ni + 2Sr/W–Zr	65.48	59.53	9.09
5Ni + 3Sr/W–Zr	56.12	51.88	7.56

^aafter 30 min on-stream; ^bafter 450 min on-stream; ^cD.F. = (Initial CH₄ conversion — Final CH₄ conversion) × 100/Initial CH₄ conversion

catalyst has the highest intensity strong basic sites. It may be due to the stabilization of bonded carbonate species by large-size Sr^{+2} cation over the catalyst surface [39]. The role of such CO_2 -stabilized surface species may be crucial in enducing DRM reaction over the catalyst surface. $5\text{Ni} + 3\text{Sr}/\text{W}-\text{Zr}$ catalyst had a wide distribution of basic sites from weak to very strong range. Finally, very strong basic sites (about 700°C) over $5\text{Ni} + 3\text{Sr}/\text{W}-\text{Zr}$ is constituted by thermally stable carbonates [28]. The thermally stable carbonates may not release CO_2 , or it may be decomposed into successive intermediates for oxidation of carbon deposit during DRM. It may affect the catalytic activity adversely. The excessive basicity of the $5\text{Ni} + 3\text{Sr}/\text{W}-\text{Zr}$ catalyst might promote the Boudouard reaction ($2\text{CO} \rightleftharpoons \text{C} + \text{CO}_2$), due to equilibrium considerations at high temperatures, resulting in a greater amount of carbon deposited on the catalyst's surface [21, 40].

Fourier transform infrared spectroscopy (FTIR)

To understand the different types of CO_2 -interacting species over the catalyst surface, the FTIR spectra of fresh and reduced $5\text{Ni} + x\text{Sr}/\text{W}-\text{Zr}$ ($x=0, 1, 2,$ and 3) catalyst system are taken in $1000\text{--}1800\text{ cm}^{-1}$ range (Fig. 4). It is clearly noticeable that the bending vibration of OH (about 1630 cm^{-1}) is intensified after reduction of catalyst [41]. This observation can be understood. During reduction, H_2 is adsorbed over

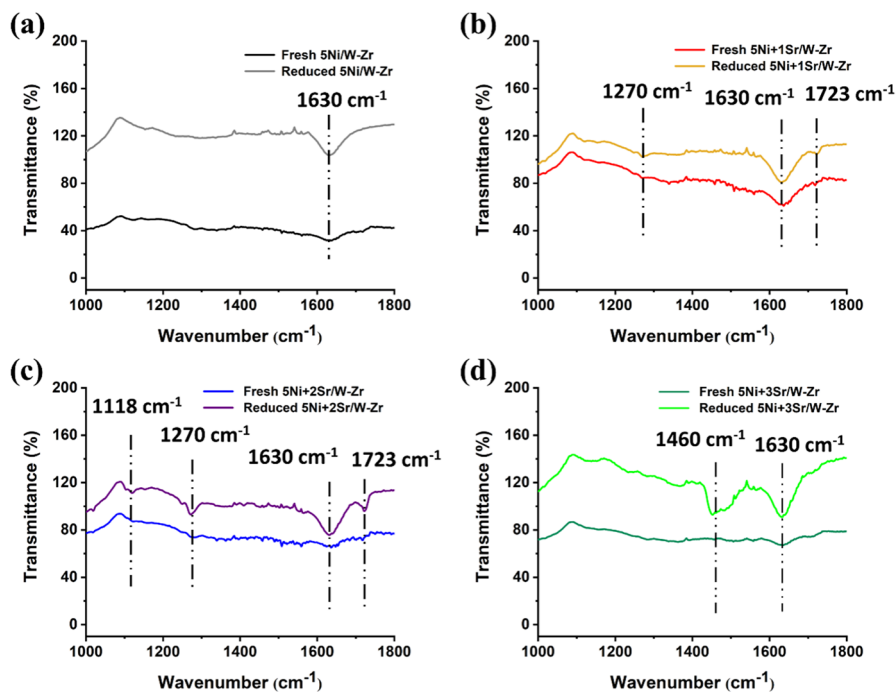


Fig. 4 FTIR results of **a** Fresh $5\text{Ni}/\text{W}-\text{Zr}$ and Reduced- $5\text{Ni}/\text{W}-\text{Zr}$ **b** Fresh $5\text{Ni} + 1\text{Sr}/\text{W}-\text{Zr}$ and Reduced- $5\text{Ni} + 1\text{Sr}/\text{W}-\text{Zr}$ **c** Fresh $5\text{Ni} + 2\text{Sr}/\text{W}-\text{Zr}$ and Reduced- $5\text{Ni} + 2\text{Sr}/\text{W}-\text{Zr}$ **d** Fresh $5\text{Ni} + 3\text{Sr}/\text{W}-\text{Zr}$ and Reduced- $5\text{Ni} + 3\text{Sr}/\text{W}-\text{Zr}$

the catalyst surface, surface oxide is reduced, and water formed over the catalyst surface. So, the bending vibration peak of OH (about 1630 cm^{-1}) is intensified after the reduction of the catalyst. After the promotional addition of 1wt% Sr addition, the diffuse vibration peaks for bidentate CO_2 -adsorbed species about 1270 cm^{-1} and 1730 cm^{-1} are observed over reduced-5Ni + 1Sr/W-Zr [41–43]. The vibration peaks for bidentate CO_2 -adsorbed species are intensified upon 2wt% Sr loading (over reduced-5Ni + 1Sr/W-Zr catalyst). Interestingly, over reduced Ni + 3Sr/W-Zr catalyst, the vibration peak of bidentate CO_2 -adsorbed species disappeared, but broad peaks for ionic carbonate (CO_3^{2-}) at $1460 \pm 10\text{ cm}^{-1}$ [43–45] appeared. Ionic carbonate makes strong interaction with large-size Sr^{2+} and forms stable carbonate over reduced 5Ni + 3Sr/W + Zr. The FTIR results also justify the result of CO_2 -TPD. J. Hong et al. [46] explained the formation of SrCO_3 by Sr-rich compound in the air. As per the hygroscopic nature of SrO, SrO was readily hydrated by absorbing airborne moisture. Further, hydrated Sr-hydroxide ($\text{Sr}(\text{OH})_2 \cdot 8\text{H}_2\text{O}$) was subjected to react with CO_2 in air and forms SrCO_3 .

Results of activity

In the blank test; 0.73% CH_4 conversion, 0.74% CO_2 conversion and 0.18 H_2/CO ratio are observed at $700\text{ }^\circ\text{C}$ whereas, at $800\text{ }^\circ\text{C}$, the CH_4 conversion, CO_2 conversion and H_2/CO ratio are improved to 1.63%, 2.01% and 0.41 respectively. The thermal decomposition of CH_4 is also thermodynamically feasible during $700\text{--}800\text{ }^\circ\text{C}$ reaction temperature. After the decomposition of CH_4 , the CH_{4-x} species are oxidized by CO_2 . So, the negligible conversion observed in the blank test is thermally driven. The activities of the 5Ni- x Sr ($x=0, 1, 2,$ and $3\text{ wt}\%$) catalysts in terms of CH_4 and CO_2 conversion for the DRM reaction were determined at $700\text{ }^\circ\text{C}$ for 480 min time on stream (TOS) and are displayed in Fig. 5 a and b respectively. The catalytic activity at about $700\text{ }^\circ\text{C}$ reaction temperature was found below the

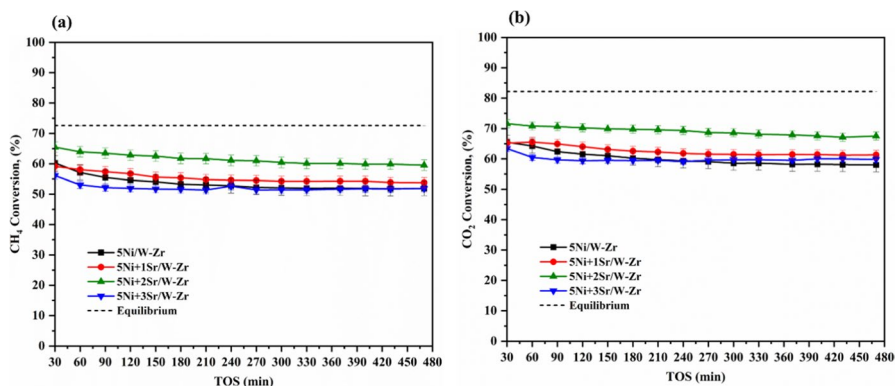


Fig. 5 CH_4 conversion (a) and CO_2 conversion versus TOS for the 5Ni + x Sr/W-Zr ($x=0, 1, 2$ and $3\text{ wt}\%$) catalysts operated at $700\text{ }^\circ\text{C}$. Experimental protocol involves three repetitions, ensuring reliable data collection, with computed standard deviations typically ranging between 1.5 and 2.5%. The error of catalytic activity is within 3% for all the experiment

thermodynamic equilibrium conversion of CH₄ and CO₂ over 5Ni–xSr ($x=0, 1, 2,$ and 3 wt%) catalysts. The conversion profiles indicate that the addition of Sr as a promoter profoundly influenced the catalytic performance. The addition of Sr promoter resulted in an increased CH₄ conversion, as demonstrated in Fig. 5a, and this conversion was found to increase with increased Sr loading percentage, except for the 5Ni + 3Sr/W–Zr catalyst sample, which showed a similar conversion compared to that of the unpromoted sample. This suggests that the 5Ni/W–Zr catalyst has an optimal loading of Sr promotion. For CO₂ conversion, comparable patterns were also observed, as shown in Fig. 5b. The reaction stoichiometry for the dry reforming of methane (DRM) involves equal conversions of CH₄ and CO₂, which results in a CH₄/CO₂ ratio of 1 and an H₂/CO ratio of 1. In practice, we often observe a deviation from this ideal scenario. The higher CO₂ conversion compared to CH₄ (CH₄/CO₂ ratio < 1) indicates that CO₂ is primarily utilized in oxidizing CH₄, consistent with DRM. However, the lower H₂/CO ratio (compared to the CH₄/CO₂ ratio) suggests that CO₂ is also involved in oxidizing H₂ via the reverse water gas shift (RWGS) reaction (CO₂ + H₂ → CO + H₂O). This phenomenon occurs due to the thermodynamic feasibility of RWGS under DRM conditions. As CH₄ serves as the source of H₂ while both CH₄ and CO₂ contribute to CO production, the H₂/CO ratio is inherently lower than the CH₄/CO₂ ratio (Fig. S1). Overall, the percentages of CO₂ conversions were larger than those of CH₄ conversions over all catalysts. This can be attributed to the simultaneous occurrence of the reverse water gas shift reaction (CO₂ + H₂ ⇌ CO + H₂O), in which the CO₂ combines with the created H₂ to produce water and CO. Overall, with initial CH₄ and CO₂ conversions of 65.5 and 71.6%, respectively, the 5Ni + 2Sr/W–Zr catalyst performed the best.

Temperature programmed oxidation (O₂–TPO)

The development of coke, which gradually inhibits the catalyst's active sites, is one potential factor that could cause the catalyst's activity to decrease throughout the methane dry reforming reaction [39]. O₂–TPD was carried out to investigate the deposited carbon.

While the CO₂ amount evolved during the oxidation allows for quantitative comparison, the T_{max} observed in TPO curves may indicate the carbon binding strength to the catalyst surface. It also reflects the kinetics of the carbon-burning process. The TPO peaks below 450 °C, 450–550 °C and above 600 °C were categorized as amorphous carbon, carbon nanotube and inert carbon, respectively [13]. The TPO thermogram of all the catalysts utilized, as shown in Fig. 6 (a), reveals a single exothermic peak with a T_{max} of about 650 °C [39, 47]. So, the TPO peak of about 650 °C is recognized as an inert carbon deposit that causes catalyst deactivation. Interestingly, the 5Ni/W–Zr promotion with 2.0 wt% of Sr shows the lowest O₂–TPO peak intensity which signs the presence of the minimum amount of inert carbon deposit. This later observation is in line with the previously discussed trend in catalytic activity, which showed that Ni-based catalysts with only 2.0 weight percent of Sr had the best catalytic performance and the least amount of catalytic activity loss when compared to other catalyst samples.

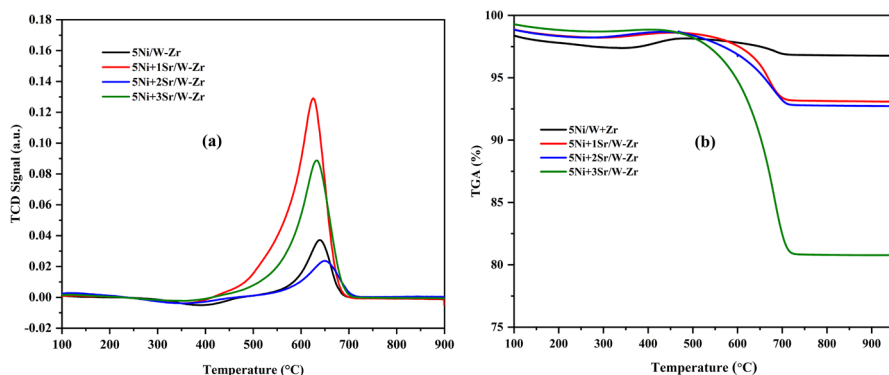


Fig. 6 TPO (a) and TGA (b) profiles for the Ni- x Sr/W-Zr ($x=0, 1.0, 2.0,$ and 3 wt. %) spent catalysts after TOS of 450 min, at 700 °C and 1 atm

Thermogravimetric analysis (TGA)

The TGA analysis of the used catalysts is illustrated in Fig. 6b. As can be seen from the figure, for all catalyst samples, the weight loss commenced beyond the temperature of 500 °C, following TPO results, which is due to the burning of the deposited coke that inhibits the catalytic activity. Moreover, the TGA analysis reveals that the percentage of deposited coke over the unpromoted Ni/W-Zr catalyst was the lowest, with only about 2.5 wt%. This may be attributable to the unpromoted catalyst's relatively lower activity than promoted ones.

Conversely, the incorporation of Sr showed a significant effect on coke formation. Specifically, the deposited coke was found to increase with increased Sr content, which is an expected trend due to enhanced activity on Sr promotion. The percentages of coke deposited were about 6.9, 7.3, and 19.2 wt% for 1, 2, and 3 wt% of Sr loading. O₂-TPO results show the oxidation of carbon deposit over 5Ni + 2Sr/W-Zr is minimum, whereas TGA results show the weight loss over 5Ni + 2Sr/W-Zr is average. The different results of TGA than TPO can be understood. The net weight loss under TGA is the combined contribution of weight loss (due to oxidation of carbon deposit) as well as weight gain (due to oxidation of metal into their higher oxides). So, O₂-TPO results are more reliable than TGA in mean of the carbon deposit study.

TEM analysis

The TEM micrographs for the fresh unpromoted (5Ni/W-Zr) and Sr promoted (5Ni + 2Sr/W-Zr) catalyst samples are shown in Fig. 7 a and b, while that of used samples after the catalytic reaction at 700 °C are shown in Fig. 7c and d, respectively. Due to agglomerate formation at high temperatures, the nickel tendency of sintering is obvious and can be seen in both cases, before and after the reaction. However, it can be noticed that after the DRM reaction, the Ni particles sintering

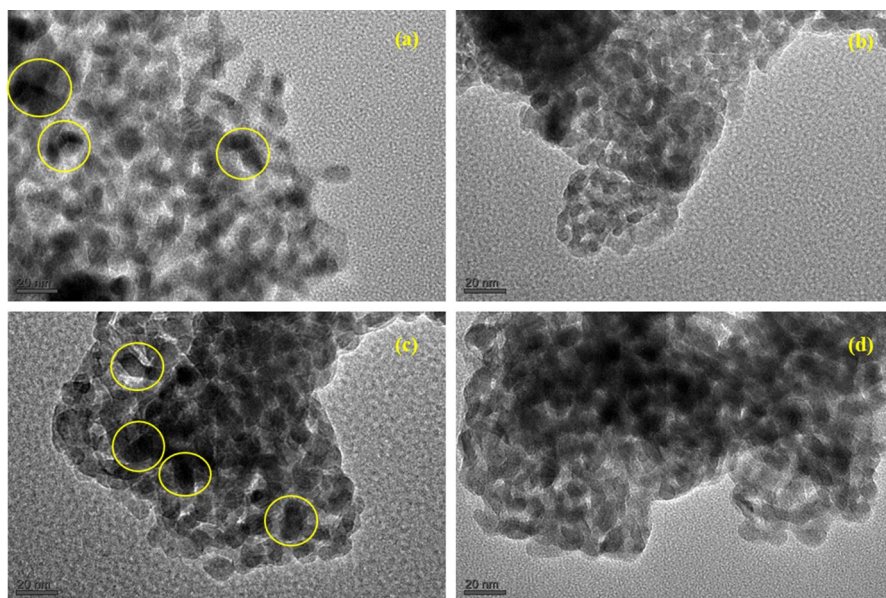


Fig. 7 TEM micrographs of fresh **a** Ni/W–Zr and **b** Ni+2Sr/W–Zr, and used **c** Ni/W–Zr and **d** Ni+Sr/W–Zr catalysts after catalytic reaction at $T_R = 700\text{ }^\circ\text{C}$

becomes more prominent, shown as dark spots and highlighted by circles. On the other hand, it can also be noticed that the nickel particles appear to be relatively well-dispersed and uniform in size after Sr promotion, indicated by the appearance of less number and smaller size of the dark spots, as shown in Fig. 7(d). This later observation implies that the incorporated Sr promoter stabilizes Ni particles against clustering under severe DRM conditions.

Raman analysis

Figure 8 illustrates the Raman spectra of the spent catalysts; the aim was to get better insights into the nature of carbon deposits onto the spent catalysts and their graphitization characteristics. As can be observed, the Raman spectra of spent catalysts showed two intense peaks at the Raman shift of 1350 cm^{-1} and 1589 cm^{-1} , corresponding to the D and G bands, respectively. The former refers to the imperfections due to carbon disorder of amorphous carbon deposits (D–band), whereas the latter is attributed to the vibration of neighboring carbon atoms of ordered graphitic carbon (G–band). Apart from the D and G bands, The Raman band at 2170 cm^{-1} and 2400 cm^{-1} are also observed as un-promoted catalysts (5Ni/W–Zr). In literature, the band at 2175 cm^{-1} is reported to stretching the vibration of carbyne [48]. The band at 2450 cm^{-1} is actually the first overtone of a Raman-inactive graphitic lattice vibration mode at $\sim 1220\text{ cm}^{-1}$ (D'' band), and so this band is shown by 2D'' [49].

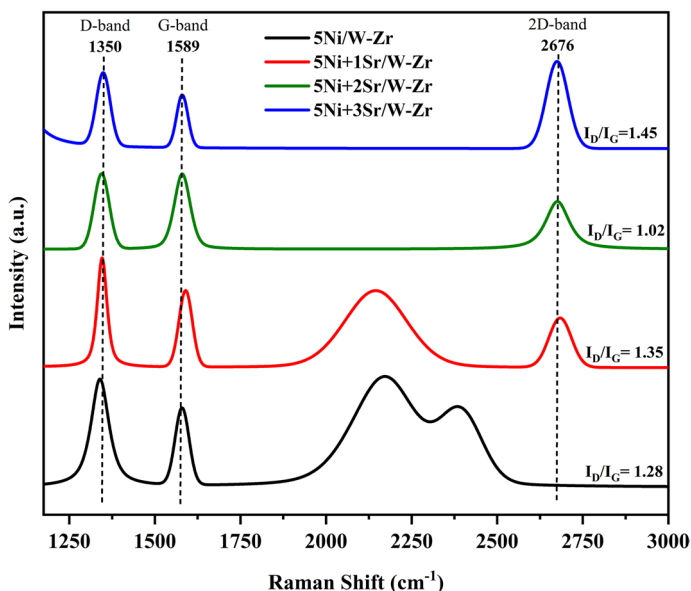


Fig. 8 Raman spectra of used catalysts after 470 min TOS in DRM, at 700 °C and 1 atm

So, it can be said that a diverse array of carbon deposits are present over the unpromoted catalyst than the rest catalyst.

Interestingly, upon 1wt% Sr loading, the 2D'' band disappeared, and a new band, about 267 cm^{-1} for the 2D-band, appeared [50]. Upon further loading of Sr (2–3 wt%), the Raman band for carbyne-like carbon species is disappeared. 5Ni + 2Sr/W-Zr and 5Ni + 3Sr/W-Zr catalysts have a D band, G band and 2D band. The intensity ratio of the D-band to the G-band (I_D/I_G) is a very important factor frequently used as a measure of the degree of disorder or structural defects in the carbonaceous samples. Promotion of the 5Ni/W-Zr catalyst with Sr resulted in increased I_D/I_G value; this value increased nominally from 1.28 to 1.45 on increased loading of Sr promoter, except for the 5Ni + 2Sr/W-Zr sample, which showed the least value of I_D/I_G ratio of 1.02. This indicates that the 5Ni + 2Sr/W-Zr sample had the highest degree of graphitization.

Discussion

By correlating collective information from different characterization techniques, the physio-chemical properties of the catalyst surface can be speculated. The possible reaction mechanism over each catalyst system is presented in Fig. 9. DRM reaction is initiated by the decomposition of CH_4 into CH_{4-x} ($x = 1-4$) over catalytic active metallic Ni. Further, there is a competition between CH_{4-x} oxidation by CO_2 as well as CH_{4-x} polymerization (shown by step 1 and step 2 in Fig. 9).

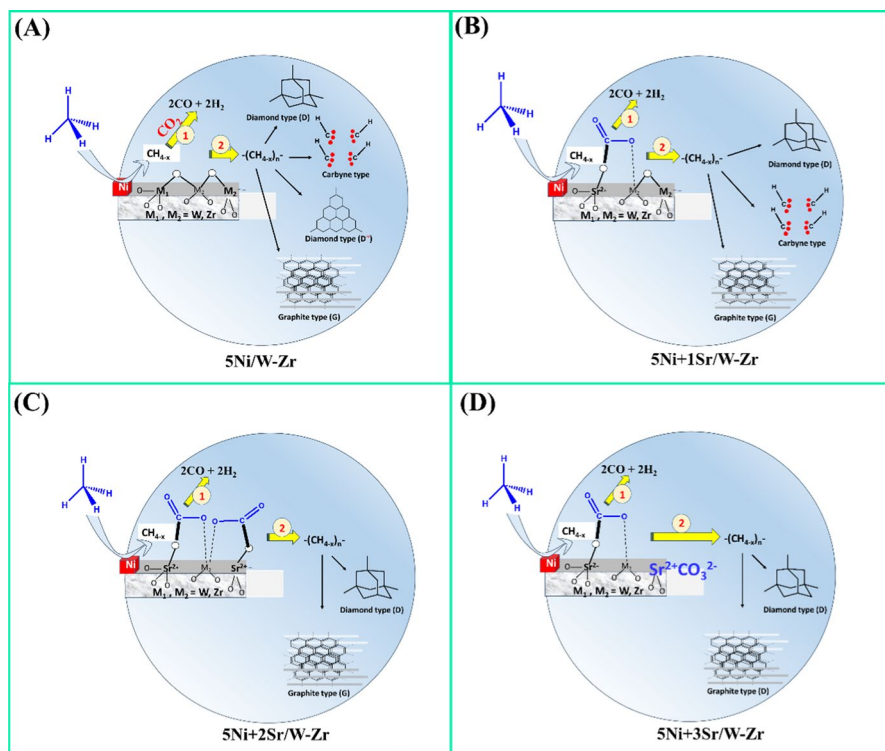


Fig. 9 Reaction over catalyst after decomposition of CH_4 into CH_{4-x} ($x=1-4$) over metallic Ni. **A** 5Ni/W-Zr catalyst: (1) oxidation of CH_{4-x} by CO_2 (into syngas) (2) polymerization of CH_{4-x} into diamond, carbyne, graphene and graphite type carbon. **B** 5Ni+1Sr/W-Zr catalyst: (1) oxidation of CH_{4-x} by interacted- CO_2 (through Sr^{2+}) species into CO_2 (2) CH_{4-x} polymerization into diamond, carbyne and graphite type carbon. **C** 5Ni+2Sr/W-Zr catalyst: (1) oxidation of CH_{4-x} is frequently by interacted- CO_2 (through Sr^{2+}) species into CO_2 (2) polymerization of CH_{4-x} into diamond and graphite type carbon. **D** 5Ni+3Sr/W-Zr catalyst: (1) Oxidation CH_{4-x} is perturbed by thermally stable CO_2 -interacting species/carbonate (through Sr^{2+}) species (2) CH_{4-x} oligomerizes to diamond and graphite type carbon

The Earlier one results into syngas formation, as well as the latter results into carbon deposit formation.

Over 5Ni/W-Zr and 5Ni+1Sr/W-Zr catalyst, the reducibility profile and basicity profile are not much different. O_2 -TPO study shows that there is a huge difference in the carbon oxidation profiles of both catalysts. The intensity of the oxidizing carbon peak in 5Ni+1Sr/W-Zr is the highest among the rest catalysts. The Raman profile shows the absence of 2D'' carbon peak over 5Ni+1Sr/W-Zr whereas the 5Ni/W-Zr catalyst surface has all four types of carbon deposits, namely diamond (D), carbyne, 2D'' and graphite (G) type carbon (Fig. 9 A and B). So, a more diverse array of carbon deposits are present over unpromoted catalysts than 5Ni+1Sr/W-Zr. The catalytic activity (CH_4 conversion) result of both

catalysts remains between 52 and 54% during 470-min TOS. Due to huge carbon deposit, the progress in catalytic activity over the 5Ni + 1Sr/W–Zr catalyst is not much more impressive than an unpromoted catalyst.

Upon 2wt% Sr loading over 5Ni/W–Zr, the basicity pattern improved intensively in the strong basic sites region, which is known for Sr²⁺ mediated interaction of CO₂ species over the catalyst surface (Fig. 9 C). The wide interaction of CO₂ results in the profound oxidation of carbon deposits. It causes the lowest amount of inert carbon deposit over 5Ni + 2Sr/W–Zr catalyst. In carbon type, the 5Ni + 2Sr/W–Zr catalyst has the deposition of diamond and graphitic type carbon deposition. In total, the wide interaction of CO₂ vis-à-vis potential oxidation of carbon deposit over the catalyst surface results in the best catalytic activity toward DRM. 5Ni + 2Sr/W–Zr catalyst acquired about 60% CH₄ conversion at the end of 470-min.

Upto 3wt% Sr addition over the 5Ni/W–Zr catalyst, the very strong basic sites are generated (according to CO₂-TPD), which is known for thermally stable carbonated (Fig. 9 D). The thermally stable carbonate species may not undergo further decomposition for subsequent oxidation of carbon deposits. It may be one of the regions of inferior catalytic activity. The carbon types over spent 5Ni + 2Sr/W–Zr and 5Ni + 3Sr/W–Zr catalyst are similar. The catalyst just shows ~52% CH₄ conversion (which is very similar to an unpromoted catalyst) up to 470 min TOS.

Conclusion

In this study, we investigated the impact of Sr promotion on the catalytic performance of 5Ni–W–Zr catalysts for dry methane reforming. Different loadings of Sr promoter, ranging from 0 to 3 wt%, were prepared and extensively characterized both before and after the DRM reaction. The characterization results of the as-prepared catalysts indicated that the addition of Sr did not alter the mesoporous structure of the catalysts, as evidenced by the BET results. Moreover, the H₂-TPR analysis revealed an improvement in catalyst reducibility due to Sr incorporation, while the CO₂-TPD analysis demonstrated an increase in the catalyst's basicity, leading to enhanced and stable CO₂ adsorption. Among the various Sr loadings, the catalyst with 2.0 wt% Sr promoter over 5Ni/W–Zr catalyst has improved basicity in strong basic sites region (attributed to Sr²⁺ mediated interaction of CO₂ species) and potential oxidation of carbon deposit which results into highest CH₄ and CO₂ conversions at the reaction temperature of 700 °C. Additionally, the presence of the Sr promoter influenced the type of carbon produced during the reaction. Unpromoted catalyst has diamond (D, 2D''), graphitic (G) and carbyne-type carbon deposit. 5Ni + 1Sr/W–Zr has lack of 2D'' carbon but appearance of 2D carbon. ≥2wt%Sr over 5Ni/W–Zr retains only D, G and 2D carbon. These findings contribute to a better understanding of the role of Sr promotion in dry methane reforming and understanding of the organization of different types of carbon deposits over the catalyst surface.

Supplementary Information The online version contains supplementary material available at <https://doi.org/10.1007/s11164-023-05210-4>.

Acknowledgements The Deputyship for Research & Innovation, Ministry of Education in Saudi Arabia, for funding this research work through the Project number (IFKSUOR3-075-8). RK acknowledge Indus University, Ahmedabad, for supporting research. Dr Ahmed I. Osman wishes to acknowledge the support of The Bryden Center project (Project ID VA5048), which was awarded by The European Union's INTERREG VA Programme and managed by the Special EU Programs Body (SEUPB).

Author contributions AYE contributed to Methodology, Investigation, Data curation, Writing—original draft., AHF contributed to Conceptualization, Review, Data curation, Validation, Software, Methodology, Formal analysis. AAI contributed to Methodology, Funding acquisition, Project Administration, Formal analysis, Data curation, Reviewing. AIO contributed to Conceptualization, Data curation, Visualization, Software, Methodology, Formal analysis. AEA contributed to Funding acquisition, Data curation, Conceptualization, Investigation, Software, Methodology, Formal analysis. SFA contributed to Data curation, Conceptualization, Investigation, Software, Methodology, Formal analysis. RK contributed to Data curation, Conceptualization, Writing—review & editing. ASAF contributed to Data curation, Conceptualization, Writing—review & editing.

Funding The Deputyship for Research & Innovation, Ministry of Education in Saudi Arabia, for funding this research work through the Project number (IFKSUOR3-075-8).

Data availability The authors confirm that the data supporting the findings of this study are available within the article and its supplementary materials.

Declarations

Conflict of interest The authors declare no competing interests.

Ethical approval Not applicable.

Open Access This article is licensed under a Creative Commons Attribution 4.0 International License, which permits use, sharing, adaptation, distribution and reproduction in any medium or format, as long as you give appropriate credit to the original author(s) and the source, provide a link to the Creative Commons licence, and indicate if changes were made. The images or other third party material in this article are included in the article's Creative Commons licence, unless indicated otherwise in a credit line to the material. If material is not included in the article's Creative Commons licence and your intended use is not permitted by statutory regulation or exceeds the permitted use, you will need to obtain permission directly from the copyright holder. To view a copy of this licence, visit <http://creativecommons.org/licenses/by/4.0/>.

References

1. A. Abdulrasheed, A. Abdul, Y. Gambo, M. Ibrahim, H. Umar, M. Yusuf, S. Hamid, *Renew. Sustain. Energy Rev.* **108**, 175 (2019)
2. B. Abdullah, N.A. Abdghani, D.V.N. Vo, *J. Clean. Prod.* **162**, 170 (2017)
3. X.S. Zhao, G.Q. Lu, G.J. Millar, *Ind. Eng. Chem. Res.* **35**, 2075 (1996)
4. X.U. Yan, X. Du, L.I. Jing, W. Peng, Z.H.U. Jie, F. Ge, Z. Jun, S. Ming, W. Zhu, *J. Fuel Chem. Technol.* **47**, 199 (2019)
5. L. Zhou, L. Li, N. Wei, J. Li, J. Basset, *ChemCatChem* **7**, 2508 (2015)
6. L. Qin, Z. Hu, M. Hu, B. Zhao, L. Kong, W. Chen, J. Han, *Int. J. Hydrogen Energy* **48**, 13442 (2023)
7. S. Sokolov, E.V. Kondratenko, M.M. Pohl, U. Rodemerck, *Int. J. Hydrogen Energy* **38**, 16121 (2013)
8. Q.L.M. Ha, U. Armbruster, H. Atia, M. Schneider, H. Lund, G. Agostini, J. Radnik, H.T. Vuong, A. Martin, *Catalysts* **7**, 157 (2017)
9. Z. Alipour, M. Rezaei, F. Meshkani, *Fuel* **129**, 197 (2014)
10. Y. Ramezani, F. Meshkani, M. Rezaei, *Int. J. Hydrogen Energy* **43**, 22347 (2018)

11. A.S. Al-Fatesh, S.O. Kasim, A.A. Ibrahim, A.I. Osman, A.E. Abasaheed, H. Atia, U. Armbruster, L. Frusteri, A. Bin Jumah, Y.M. Alanazi, *Fuel* **330**, 125523 (2022)
12. X. Yan, T. Hu, P. Liu, S. Li, B. Zhao, Q. Zhang, W. Jiao, S. Chen, P. Wang, J. Lu, *Appl. Catal. B* **246**, 221 (2019)
13. A.S. Al-Fatesh, Y. Arafat, S.O. Kasim, A.A. Ibrahim, A.E. Abasaheed, A.H. Fakeeha, *Appl. Catal. B* **280**, 119445 (2021)
14. O. Gamba, S. Moreno, R. Molina, *Int. J. Hydrogen Energy* **36**, 1540 (2011)
15. T. Zhang, Z. Liu, Y.-A. Zhu, Z. Liu, Z. Sui, K. Zhu, X. Zhou, *Appl. Catal. B* **264**, 118497 (2020)
16. J. Sarkar, S. Bhattacharyya, *Arch. Thermodyn.* **33**, 23 (2012)
17. N.A.K. Aramouni, J.G. Touma, B.A. Tarboush, J. Zeaiter, M.N. Ahmad, *Renew. Sustain. Energy Rev.* **82**, 2570 (2018)
18. A. Chatla, I.W. Almanassra, P. Kallem, M.A. Atieh, H. Alawadhi, V. Akula, F. Banat, *J. CO2 Utilization* **62**, 102082 (2022)
19. S. Azeem, R. Aslam, and M. Saleem, *Int. J. Chem. Eng.* 2022, (2022).
20. A.S. Al-Fatesh, R. Patel, V.K. Srivastava, A.A. Ibrahim, M.A. Naeem, A.H. Fakeeha, A.E. Abasaheed, A.A. Alquraini, R. Kumar, *ACS Omega* **7**, 16468 (2022)
21. A.H. Fakeeha, A. Kurdi, Y.A. Al-Baqmaa, A.A. Ibrahim, A.E. Abasaheed, A.S. Al-Fatesh, *Energies* **15**, 3841 (2022)
22. Y. Dai, R. Zou, T. Ba, J. Zhang, C. Ju Nliu, *J. CO2 Utilization* **51**, 101647 (2021)
23. A. Wolfbeisser, O. Sophiphun, J. Bernardi, J. Wittayakun, K. Föttinger, G. Rupprechter, *Catal. Today* **277**, 234 (2016)
24. A. Kambolis, H. Matralis, A. Trovarelli, C. Papadopoulou, *Appl. Catal. A* **377**, 16 (2010)
25. V. García, J.J. Fernández, W. Ruíz, F. Mondragón, A. Moreno, *Catal. Commun.* **11**, 240 (2009)
26. J. Titus, T. Roussi ere, G. Wasserschaff, S. Schunk, A. Milanov, E. Schwab, G. Wagner, O. Oeckler, and R. Gl aser, *Catal. Today* (2015).
27. Y. Lou, M. Steib, Q. Zhang, K. Tiefenbacher, A. Horv ath, A. Jentys, Y. Liu, J.A. Lercher, *J. Catal.* **356**, 147 (2017)
28. R. Patel, A.S. Al-Fatesh, A.H. Fakeeha, Y. Arafat, S.O. Kasim, A.A. Ibrahim, S.A. Al-Zahrani, A.E. Abasaheed, V.K. Srivastava, R. Kumar, *Int. J. Hydrogen Energy* **46**, 25015 (2021)
29. A.E. Abasaheed, M.S. Lanre, S.O. Kasim, A.A. Ibrahim, A.I. Osman, A.H. Fakeeha, A. Alkhalifa, R. Arasheed, F. Albaqi, N.S. Kumar, W.U. Khan, R. Kumar, F. Frusteri, A.S. Al-Fatesh, A.A. Bagabas, *Int. J. Hydrogen Energy* **48**, 26492 (2022)
30. N.D. Charisiou, G. Siakavelas, K.N. Papageridis, A. Baklavaridis, L. Tzounis, G. Goula, I.V. Yentekakis, K. Polychronopoulou, M.A. Goula, *Front. Environ. Sci.* **5**, 1 (2017)
31. J.C. Yori, J.M. Parera, *Catal. Lett.* **65**, 205 (2000)
32. A.A. Ibrahim, A.H. Fakeeha, A.E. Abasaheed, A.S. Al-Fatesh, *Catalysts* **11**, 827 (2021)
33. M. Zinkevich, *J. Solid State Chem.* **178**, 2818 (2005)
34. A.H. Fakeeha, M.A. Naeem, W.U. Khan, A.S. Al-Fatesh, *J. Ind. Eng. Chem.* **20**(2), 549 (2014)
35. J. Yan, D. Yu, P. Sun, H. Huang, Cuihua Xuebao/Chin. J. Catal. **32**, 405 (2011)
36. A. Bermejo-L opez, B. Pereda-Ayo, J.A. Onrubia-Calvo, J.A. Gonz alez-Marcos, J.R. Gonz alez-Velasco, *J. CO2 Utilization* **58**, 101922 (2022)
37. X. Huang, W. Mo, X. He, X. Fan, F. Ma, D. Tax, *ACS Omega* **6**, 16381 (2021)
38. L. Chen, Z. Qi, S. Zhang, J. Su, and G. A. Somorjai, *Catalysts* **10**, 858 (2020)
39. F. Miccio, A.N. Murri, E. Landi, *Ind. Eng. Chem. Res.* **55**, 6696 (2016)
40. M.A.A. Aziz, A.A. Jalil, S. Wongsakulphasatch, D.V.N. Vo, *Catal. Sci. Technol.* **10**, 35 (2020)
41. J. Khatri, A.H. Fakeeha, S.O. Kasim, M.S. Lanre, A.E. Abasaheed, A.A. Ibrahim, R. Kumar, A.S. Al-Fatesh, *Int. J. Energy Res.* **45**, 19289 (2021)
42. L. Vlaev, D. Damyanov, M.M. Mohamed, *Coll. Surf.* **36**, 427 (1989)
43. G. Busca, V. Lorenzelli, *Mater. Chem.* **7**, 89 (1982)
44. R.P. Turcotte, J.O. Sawyer, L. Eyring, *Inorg. Chem.* **8**, 238 (1969)
45. J. Khatri, A.S. Al-Fatesh, A.H. Fakeeha, A.A. Ibrahim, A.E. Abasaheed, S.O. Kasim, A.I. Osman, R. Patel, R. Kumar, *Mol. Catal.* **504**, 111498 (2021)
46. J. Hong, S.J. Heo, P. Singh, Water mediated growth of oriented single crystalline SrCO3 nanorod arrays on strontium compounds. *Sci. Rep.* **11**(1), 3368 (2021)
47. A.S. Al-Fatesh et al., *Energy Sci. Eng.* **11**(10), 3780 (2023)
48. B. Pan, J. Xiao, J. Li, P. Liu, C. Wang, G. Yang, *Sci. Adv.* **1**, 1 (2015)
49. N.D. Charisiou, L. Tzounis, V. Sebastian, S.J. Hinder, M.A. Baker, K. Polychronopoulou, M.A. Goula, *Appl. Surf. Sci.* **474**, 42 (2019)

50. A. Horváth, G. Stefler, O. Geszti, A. Kienneman, A. Pietraszek, L. Guzzi **169**, 102 (2011)

Publisher's Note Springer Nature remains neutral with regard to jurisdictional claims in published maps and institutional affiliations.